Modeling Hybrid Automotive Systems with the POG Technique

Roberto Zanasi
Information Engineering Department
University of Modena e Reggio Emilia
Via Vignolese 905, Modena, Italy
roberto.zanasi@unimore.it

Federica Grossi
Information Engineering Department
University of Modena e Reggio Emilia
Via Vignolese 905, Modena, Italy
federica.grossi@unimore.it

***Abstract*—In this paper the Power-Oriented Graphs (POG) technique is used for modeling planetary gears and hybrid automotive systems. The POG technique allows to graphically describe the dynamic model of any type of physical system (in different energetic domains) putting in evidence the power flows within the modeled systems. The POG schemes are easy to use, easy to understand even by a neophyte and can be directly implemented in Simulink. Because of the POG modular structure, complex physical systems can be modeled by composing subsystems models. Following this approach a whole power-split hybrid vehicle is modeled, starting from modeling its main subsystems: planetary gear, internal combustion engine, multi-phase synchronous motor and vehicle dynamics. Simulation results of the modeled hybrid system end the paper.**

I. Introduction

The analysis of the dynamic behavior of hybrid electric vehicles is nowadays a very important topic, especially aiming at reducing fuel consumption and exhaust emissions. This paper deals with power-split propulsion system of hybrid electric vehicles, in particular the one equipped with an internal combustion engine and a multi-phase synchronous machine, where the power split is carried out by means of a planetary gear system. In this paper the Power-Oriented Graphs (POG) modeling technique is exploited to provide the models of the considered dynamic systems: a planetary gear with internal elasticity and dissipation, a multi-phase permanent magnet synchronous motor and a power-split hybrid vehicle. The paper is organized as follows: Sec. II describes the basic properties of the POG modeling technique; Sec. III, IV and V show, respectively, the POG dynamic models of planetary gears, electric motor and of the hybrid propulsion system; in Sec. VI some simulation results are reported.

II. Power-Oriented Graphs basic principles

The Power-Oriented Graphs technique [7] is suitable for modeling physical systems. The POG block schemes are normal block diagrams combined with a particular modular structure based on the use of the two blocks shown in Fig. 1.a and Fig. 1.b: the *elaboration block* (e.b.) stores and/or dissipates energy (i.e. springs, masses, dampers, capacities, inductances, resistances, etc.); the *connection block* (c.b.) redistributes the power within the system without storing nor dissipating energy (i.e. gears, transformers, etc.). The e.b. and the c.b. are suitable for representing both scalar and vectorial systems. In the vectorial case, $\mathbf{G}(s)$ and $\mathbf{K}$ are matrices: $\mathbf{G}(s)$ is always a square matrix composed by positive real transfer functions; matrix $\mathbf{K}$ can also be rectangular. The circle present in the e.b. is a summation element and the black spot represents a minus sign that multiplies the entering variable. The main feature of the Power-Oriented Graphs is to keep a direct correspondence between the dashed sections of the graphs and real power sections of the modeled systems: the scalar product $\mathbf{x}^{\mathrm{T}}\mathbf{y}$ of the two *power vectors* $\mathbf{x}$ and $\mathbf{y}$ involved in each dashed line of a power-oriented graph, see Fig. 1, has the physical meaning of *the power flowing through that particular section*. The Bond Graphs technique, see [5] and [3], is based on the same idea, but it uses a different and specific graphical representation.

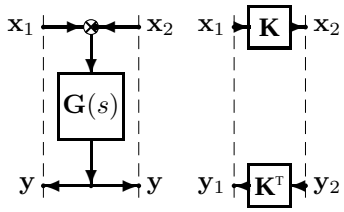

a) *e. b.* b) *c. b.*

Figure 1. POG basic blocks and variables: a) *elaboration block*; b) *connection block*.

Each Physical Element interacts with the external world through the power sections associated to its terminals. Another important property of the POG technique is the direct correspondence between POG schemes and corresponding state space dynamic equations. For example, the POG scheme shown in Fig. 2 can be represented by the state space equations (1) where *energy matrix* $\mathbf{L}$ is symmetric and positive definite: $\mathbf{L} = \mathbf{L}^{\mathrm{T}} > 0$. It can be easily shown that when $\mathbf{D} = 0$ it follows that $\mathbf{C} = \mathbf{B}^{\mathrm{T}}$. When an eigenvalue of matrix $\mathbf{L}$ tends to zero (or to infinity), system (1) degenerates towards a lower dimension dynamic system. In this case, the dynamic model of the "reduced" system, see (2), can be obtained from (1) using a simple "congruent" transformation $\mathbf{x} = \mathbf{T}\,\mathbf{z}$ where (if $\mathbf{T}$ is constant) $\overline{\mathbf{L}} = \mathbf{T}^{\mathrm{T}}\mathbf{L}\mathbf{T}$, $\overline{\mathbf{A}} = \mathbf{T}^{\mathrm{T}}\mathbf{A}\mathbf{T}$, $\overline{\mathbf{B}} = \mathbf{T}^{\mathrm{T}}\mathbf{B}$, $\overline{\mathbf{C}} = \mathbf{C}\mathbf{T}$ and $\overline{\mathbf{D}} = \mathbf{D}$. The POG scheme of Fig. 2 can also be easily input-output inverted, both graphically and mathematically, as shown in Fig. 3. In this case $\tilde{\mathbf{L}} = \mathbf{L}$, $\tilde{\mathbf{A}} = \mathbf{A} + \mathbf{B}\mathbf{D}^{-1}\mathbf{C}$, $\tilde{\mathbf{B}} = \mathbf{B}\mathbf{D}^{-1}$,

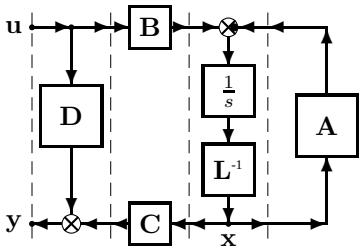

$$\begin{cases} \mathbf{L}\,\dot{\mathbf{x}} = -\mathbf{A}\,\mathbf{x} + \mathbf{B}\,\mathbf{u} \\ \mathbf{y} = \mathbf{C}\,\mathbf{x} + \mathbf{D}\,\mathbf{u} \end{cases} \tag{1}$$

$$\Downarrow (\mathbf{x} = \mathbf{T}\,\mathbf{z})$$

$$\begin{cases} \overline{\mathbf{L}}\,\dot{\mathbf{z}} = -\overline{\mathbf{A}}\,\mathbf{z} + \overline{\mathbf{B}}\,\mathbf{u} \\ \mathbf{y} = \overline{\mathbf{C}}\,\mathbf{z} + \overline{\mathbf{D}}\,\mathbf{u} \end{cases} \tag{2}$$

Figure 2. POG block scheme of a generic dynamic system.

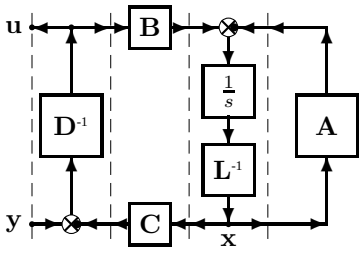

$$\begin{cases} \tilde{\mathbf{L}}\,\dot{\mathbf{x}} = -\tilde{\mathbf{A}}\,\mathbf{x} + \tilde{\mathbf{B}}\,\mathbf{y} \\ \mathbf{u} = \tilde{\mathbf{C}}\,\mathbf{x} + \tilde{\mathbf{D}}\,\mathbf{y} \end{cases} \tag{3}$$

where

$$\tilde{\mathbf{L}} = \mathbf{L}, \quad \tilde{\mathbf{B}} = \mathbf{B}\mathbf{D}^{-1},$$
$$\tilde{\mathbf{A}} = \mathbf{A} + \mathbf{B}\mathbf{D}^{-1}\mathbf{C},$$
$$\tilde{\mathbf{C}} = -\mathbf{D}^{-1}\mathbf{C}, \quad \tilde{\mathbf{D}} = \mathbf{D}^{-1}.$$

Figure 3. POG block scheme of the input-output inverted system.

$\tilde{\mathbf{C}} = -\mathbf{D}^{-1}\mathbf{C}$ and $\tilde{\mathbf{D}} = \mathbf{D}^{-1}$ are the matrices of the inverted system (3).

III. POG MODELING OF A PLANETARY GEAR

Let us consider the planetary gear in Fig. 4. The main parameters of the system are: r_s and r_p sun and planet radii; J_s, b_s, J_c, b_c, J_r and b_r inertia and linear friction coefficients of the sun, carrier and ring, respectively; K_{sc}, d_{sc}, K_{cr} and d_{cr} stiffness and friction coefficients of the sun-carrier and carrier-ring elastic elements, respectively. The extended POG dynamic model of the considered planetary gear is shown in the upper part of Fig. 5: the carrier, the planets and the ring interact each other through the two elastic elements K_{cr} and K_{sc}. The corresponding state space dynamic equations are shown in lower part of Fig. 5:

$$\overline{\mathbf{L}}\,\dot{\overline{\mathbf{x}}} = -\overline{\mathbf{A}}\,\overline{\mathbf{x}} + \overline{\mathbf{B}}\,\mathbf{u}, \qquad \mathbf{y} = \overline{\mathbf{B}}^{\mathrm{T}}\,\overline{\mathbf{x}} \tag{5}$$

A. Reduced elastic model

For certain applications the POG model of Fig. 5 can be too much detailed. In these cases it can be of interest to find some reduced models, see [11]. Using the POG reduction technique it is possible to obtain from (4) a reduced elastic model when J_s, J_c and J_r go to zero. Applying to (4) the following transformation:

$$\overline{\mathbf{x}} = \mathbf{T}_3\,\mathbf{z}, \qquad \text{where} \qquad \mathbf{T}_3 = \begin{bmatrix} 0&0&0&1&0&0 \\ 1&0&0&0&0&0 \\ 0&1&0&0&0&0 \\ 0&0&0&0&1&0 \\ 0&0&1&0&0&0 \\ 0&0&0&0&0&1 \end{bmatrix}$$

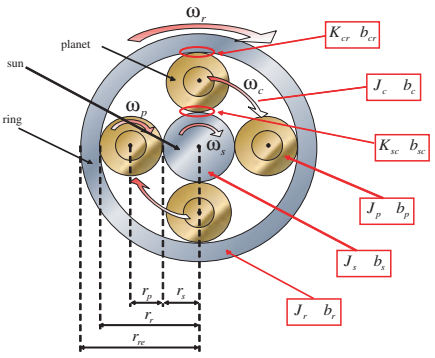

Figure 4. Planetary gear and related parameters.

and using the constraint $J_s = J_c = J_r = 0$, one obtains the following transformed system:

$$\underbrace{\begin{bmatrix} \mathbf{L}_1 & 0 \\ 0 & 0 \end{bmatrix}}_{\mathbf{L}} \underbrace{\begin{bmatrix} \dot{\mathbf{z}}_1 \\ \dot{\mathbf{z}}_2 \end{bmatrix}}_{\dot{\mathbf{z}}} = \underbrace{\begin{bmatrix} \mathbf{A}_{11} & \mathbf{A}_{12} \\ \mathbf{A}_{21} & \mathbf{A}_{22} \end{bmatrix}}_{-\mathbf{A}} \underbrace{\begin{bmatrix} \mathbf{z}_1 \\ \mathbf{z}_2 \end{bmatrix}}_{\mathbf{z}} + \underbrace{\begin{bmatrix} \mathbf{B}_1 \\ \mathbf{B}_2 \end{bmatrix}}_{\mathbf{B}} \mathbf{u}, \quad \mathbf{y} = \mathbf{C}\,\mathbf{z} + \mathbf{D}\,\mathbf{u}, \tag{6}$$

where $\mathbf{z} = \mathbf{T}_3^{\mathrm{T}}\,\overline{\mathbf{x}}$, $\mathbf{L} = \mathbf{T}_3^{\mathrm{T}}\overline{\mathbf{L}}\,\mathbf{T}_3$, $\mathbf{A} = \mathbf{T}_3^{\mathrm{T}}\overline{\mathbf{A}}\,\mathbf{T}_3$, $\mathbf{B} = \mathbf{T}_3^{\mathrm{T}}\,\overline{\mathbf{B}}$, $\mathbf{C} = [\mathbf{C}_1,\ \mathbf{C}_2] = \mathbf{B}^{\mathrm{T}} = [\mathbf{B}_1^{\mathrm{T}},\ \mathbf{B}_2^{\mathrm{T}}]$, $\mathbf{D} = 0$ and where:

$$\mathbf{z}_1 = \begin{bmatrix} F_{sc} \\ \omega_p \\ F_{cr} \end{bmatrix}, \qquad \mathbf{z}_2 = \begin{bmatrix} \omega_s \\ \omega_c \\ \omega_r \end{bmatrix}, \qquad \mathbf{L}_1 = \begin{bmatrix} \frac{1}{K_{sc}} & 0 & 0 \\ 0 & J_p & 0 \\ 0 & 0 & \frac{1}{K_{cr}} \end{bmatrix},$$

$$\mathbf{A}_{11} = \begin{bmatrix} 0 & r_p & 0 \\ -r_p & -d_{sc}r_p^2 - r_p^2 d_{cr} - b_p & -r_p \\ 0 & r_p & 0 \end{bmatrix}, \qquad \mathbf{B}_1 = \begin{bmatrix} 0&0&0 \\ 0&0&0 \\ 0&0&0 \end{bmatrix},$$

$$\mathbf{A}_{12} = \begin{bmatrix} r_s & -r_s & 0 \\ -r_s d_{sc} r_p & r_s d_{sc} r_p - r_p r_r d_{cr} & r_p r_r d_{cr} \\ 0 & r_r & -r_r \end{bmatrix}, \quad \mathbf{B}_2 = \begin{bmatrix} 1&0&0 \\ 0&1&0 \\ 0&0&1 \end{bmatrix},$$

$$\mathbf{A}_{21} = \begin{bmatrix} -r_s & -r_s d_{sc} r_p & 0 \\ r_s & r_s d_{sc} r_p - r_p r_r d_{cr} & -r_r \\ 0 & r_p r_r d_{cr} & r_r \end{bmatrix}, \qquad \mathbf{D} = \begin{bmatrix} 0&0&0 \\ 0&0&0 \\ 0&0&0 \end{bmatrix},$$

$$\mathbf{A}_{22} = \begin{bmatrix} -b_s - r_s^2 d_{sc} & r_s^2 d_{sc} & 0 \\ r_s^2 d_{sc} & -b_c - r_s^2 d_{sc} - r_r^2 d_{cr} & r_r^2 d_{cr} \\ 0 & r_r^2 d_{cr} & -b_r - r_r^2 d_{cr} \end{bmatrix}.$$

The last equation of system (6) shows the following algebraic relation between the state and input variables:

$$\mathbf{A}_{21}\,\mathbf{z}_1 + \mathbf{A}_{22}\,\mathbf{z}_2 + \mathbf{B}_2\,\mathbf{u} = 0$$

Since matrix $\mathbf{A}_{22}$ is invertible, vector $\mathbf{z}_2$ can be expressed as:

$$\mathbf{z}_2 = -\mathbf{A}_{22}^{-1}\mathbf{A}_{21}\,\mathbf{z}_1 - \mathbf{A}_{22}^{-1}\mathbf{B}_2\,\mathbf{u}$$

Applying the following rectangular transformation:

$$\mathbf{z} = \underbrace{\begin{bmatrix} \mathbf{I}_2 \\ -\mathbf{A}_{22}^{-1}\,\mathbf{A}_{21} \end{bmatrix}}_{\mathbf{T}_z} \mathbf{z}_1 + \underbrace{\begin{bmatrix} 0 \\ -\mathbf{A}_{22}^{-1}\,\mathbf{B}_2 \end{bmatrix}}_{\mathbf{T}_u} \mathbf{u}$$

to system (6) (i.e. $\mathbf{L}\,\dot{\mathbf{z}} = -\mathbf{A}\,\mathbf{z} + \mathbf{B}\,\mathbf{u}$ and $\mathbf{y} = \mathbf{C}\,\mathbf{z} + \mathbf{D}\,\mathbf{u}$), one obtains the following reduced system (note that $\mathbf{L}\,\mathbf{T}_u = 0$):

$$\begin{cases} \mathbf{T}_z^{\mathrm{T}}\mathbf{L}\,\mathbf{T}_z\,\dot{\mathbf{z}}_1 = -\mathbf{T}_z^{\mathrm{T}}\mathbf{A}\,\mathbf{T}_z\,\mathbf{z}_1 + \mathbf{T}_z^{\mathrm{T}}(\mathbf{B} - \mathbf{A}\,\mathbf{T}_u)\,\mathbf{u} \\ \mathbf{y} = \mathbf{C}\,\mathbf{T}_z\,\mathbf{z}_1 + (\mathbf{D} + \mathbf{C}\,\mathbf{T}_u)\,\mathbf{u} \end{cases}$$

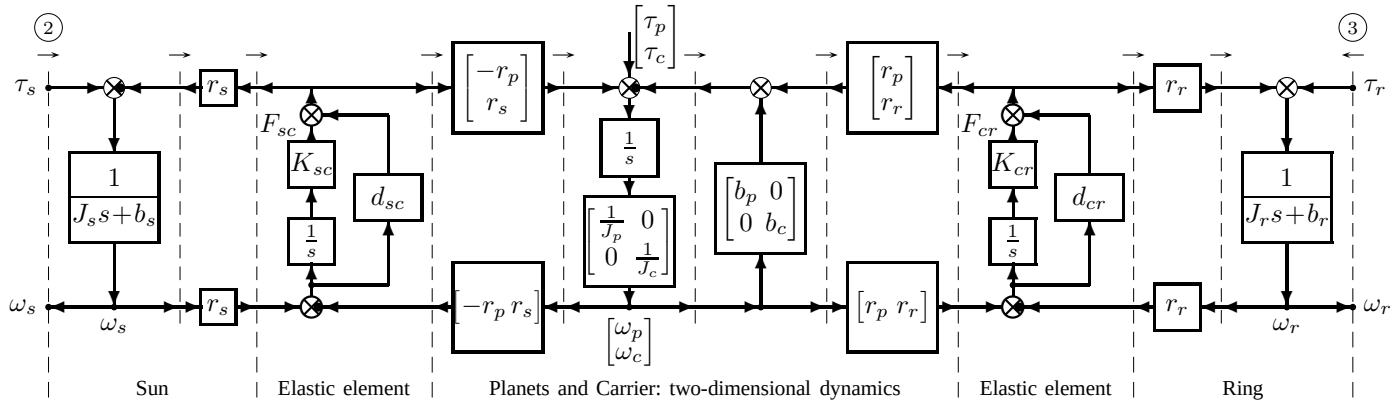

$$\underbrace{\begin{bmatrix} J_s & 0 & 0 & 0 & 0 & 0 \\ 0 & \frac{1}{K_{sc}} & 0 & 0 & 0 & 0 \\ 0 & 0 & J_p & 0 & 0 & 0 \\ 0 & 0 & 0 & J_c & 0 & 0 \\ 0 & 0 & 0 & 0 & \frac{1}{K_{cr}} & 0 \\ 0 & 0 & 0 & 0 & 0 & J_r \end{bmatrix}}_{\overline{\mathbf{L}}} \underbrace{\begin{bmatrix} \dot{\omega}_s \\ \dot{F}_{sc} \\ \dot{\omega}_p \\ \dot{\omega}_c \\ \dot{F}_{cr} \\ \dot{\omega}_r \end{bmatrix}}_{\dot{\overline{\mathbf{x}}}} = \underbrace{\begin{bmatrix} -b_s - r_s^2 d_{sc} & -r_s & -r_s d_{sc} r_p & r_s^2 d_{sc} & 0 & 0 \\ r_s & 0 & r_p & -r_s & 0 & 0 \\ -r_s d_{sc} r_p & -r_p & -b_p - d_{sc} r_p^2 - d_{cr} r_p^2 & r_s d_{sc} r_p - d_{cr} r_p r_r & -r_p & d_{cr} r_p r_r \\ r_s^2 d_{sc} & r_s & r_s d_{sc} r_p - d_{cr} r_p r_r & -b_c - r_s^2 d_{sc} - d_{cr} r_r^2 & -r_r & d_{cr} r_r^2 \\ 0 & 0 & r_p & r_r & 0 & -r_r \\ 0 & 0 & d_{cr} r_p r_r & d_{cr} r_r^2 & r_r & -b_r - d_{cr} r_r^2 \end{bmatrix}}_{-\overline{\mathbf{A}}} \underbrace{\begin{bmatrix} \omega_s \\ F_{sc} \\ \omega_p \\ \omega_c \\ F_{cr} \\ \omega_r \end{bmatrix}}_{\overline{\mathbf{x}}} + \underbrace{\begin{bmatrix} 1 & 0 & 0 \\ 0 & 0 & 0 \\ 0 & 0 & 0 \\ 0 & 1 & 0 \\ 0 & 0 & 0 \\ 0 & 0 & 1 \end{bmatrix}}_{\overline{\mathbf{B}}} \underbrace{\begin{bmatrix} \tau_s \\ \tau_c \\ \tau_r \end{bmatrix}}_{\mathbf{u}} \tag{4}$$

Figure 5. The POG block diagram and the POG state space equations of the considered planetary gear. The considered inputs are: τ_s, τ_c and τ_r.

$$\underbrace{\begin{bmatrix} \frac{1}{K_{sc}} & 0 & 0 \\ 0 & J_p & 0 \\ 0 & 0 & \frac{1}{K_{cr}} \end{bmatrix}}_{\tilde{\mathbf{L}}_e} \underbrace{\begin{bmatrix} \dot{F}_{sc} \\ \dot{\omega}_p \\ \dot{F}_{cr} \end{bmatrix}}_{\dot{\tilde{\mathbf{x}}}} = \underbrace{\begin{bmatrix} 0 & r_p & 0 \\ -r_p & -r_p^2 d_{sc} - b_p - r_p^2 d_{cr} & -r_p \\ 0 & r_p & 0 \end{bmatrix}}_{-\tilde{\mathbf{A}}_e} \underbrace{\begin{bmatrix} F_{sc} \\ \omega_p \\ F_{cr} \end{bmatrix}}_{\tilde{\mathbf{x}}} + \underbrace{\begin{bmatrix} r_s & -r_s & 0 \\ -r_s d_{sc} r_p & r_s d_{sc} r_p - r_r d_{cr} r_p & r_r d_{cr} r_p \\ 0 & r_r & -r_r \end{bmatrix}}_{\tilde{\mathbf{B}}_e} \underbrace{\begin{bmatrix} \omega_s \\ \omega_c \\ \omega_r \end{bmatrix}}_{\tilde{\mathbf{u}}}$$

$$\underbrace{\begin{bmatrix} \tau_s \\ \tau_c \\ \tau_r \end{bmatrix}}_{\tilde{\mathbf{y}}} = \underbrace{\begin{bmatrix} r_s & r_s d_{sc} r_p & 0 \\ -r_s & -r_s d_{sc} r_p + r_r d_{cr} r_p & r_r \\ 0 & -r_r d_{cr} r_p & -r_r \end{bmatrix}}_{\tilde{\mathbf{C}}_e} \underbrace{\begin{bmatrix} F_{sc} \\ \omega_p \\ F_{cr} \end{bmatrix}}_{\tilde{\mathbf{x}}} + \underbrace{\begin{bmatrix} b_s + r_s^2 d_{sc} & -r_s^2 d_{sc} & 0 \\ -r_s^2 d_{sc} & b_c + r_s^2 d_{sc} + r_r^2 d_{cr} & -r_r^2 d_{cr} \\ 0 & -r_r^2 d_{cr} & b_r + r_r^2 d_{cr} \end{bmatrix}}_{\tilde{\mathbf{D}}_e} \underbrace{\begin{bmatrix} \omega_s \\ \omega_c \\ \omega_r \end{bmatrix}}_{\tilde{\mathbf{u}}} \tag{7}$$

Figure 6. POG state space equations of the reduced planetary gear when $J_s = J_c = J_r = 0$ and the velocities are the inputs.

that in compact form is:

$$\mathbf{L}_e\, \dot{\mathbf{z}}_1 = -\mathbf{A}_e\, \mathbf{z}_1 + \mathbf{B}_e\, \mathbf{u}, \qquad \mathbf{y} = \mathbf{C}_e^{\mathrm{T}} \mathbf{z}_1 + \mathbf{D}_e^{\mathrm{T}} \mathbf{u} \tag{8}$$

where matrices $\mathbf{L}_e$, $\mathbf{A}_e$, $\mathbf{B}_e$, $\mathbf{C}_e$ and $\mathbf{D}_e$ are:

$$\begin{aligned} \mathbf{L}_e &= \mathbf{T}_z^{\mathrm{T}} \mathbf{L}\, \mathbf{T}_z = \mathbf{L}_1, \\ -\mathbf{A}_e &= -\mathbf{T}_z^{\mathrm{T}} \mathbf{A}\, \mathbf{T}_z = \mathbf{A}_{11} - \mathbf{A}_{12}\, \mathbf{A}_{22}^{-1}\, \mathbf{A}_{21}, \\ \mathbf{B}_e &= \mathbf{T}_z^{\mathrm{T}} (\mathbf{B} - \mathbf{A}\, \mathbf{T}_u) = \mathbf{B}_1 - \mathbf{A}_{12}\, \mathbf{A}_{22}^{-1}\, \mathbf{B}_2, \\ \mathbf{C}_e &= \mathbf{C}\, \mathbf{T}_z = \mathbf{C}_1 - \mathbf{C}_2\, \mathbf{A}_{22}^{-1}\, \mathbf{A}_{21}, \\ \mathbf{D}_e &= \mathbf{D} + \mathbf{C}\, \mathbf{T}_u = \mathbf{D} - \mathbf{C}_2\, \mathbf{A}_{22}^{-1}\, \mathbf{B}_2. \end{aligned}$$

Since matrix $\mathbf{D}_e$ is invertible, system (8) can be input-output inverted using the relations shown in Fig. 3. The state space equations $\tilde{\mathbf{L}}_e\, \dot{\tilde{\mathbf{x}}} = -\tilde{\mathbf{A}}_e\, \tilde{\mathbf{x}} + \tilde{\mathbf{B}}_e\, \tilde{\mathbf{u}}$ and $\tilde{\mathbf{y}} = \tilde{\mathbf{C}}_e\, \tilde{\mathbf{x}} + \tilde{\mathbf{D}}_e\, \tilde{\mathbf{u}}$ of the inverted-reduced system are shown in (7) in Fig. 6 where:

$$\tilde{\mathbf{L}}_e = \mathbf{L}_e, \quad \tilde{\mathbf{A}}_e = \mathbf{A}_e + \mathbf{B}_e \mathbf{D}_e^{-1} \mathbf{C}_e, \quad \tilde{\mathbf{B}}_e = \mathbf{B}_e \mathbf{D}_e^{-1}, \quad \tilde{\mathbf{C}}_e = -\mathbf{D}_e^{-1} \mathbf{C}_e,$$

$$\tilde{\mathbf{x}} = \mathbf{z}_1, \quad \tilde{\mathbf{u}} = \mathbf{y} = [\omega_s, \omega_c, \omega_r]^{\mathrm{T}}, \quad \tilde{\mathbf{y}} = \mathbf{u} = [\tau_s, \tau_c, \tau_r]^{\mathrm{T}}, \quad \tilde{\mathbf{D}}_e = \mathbf{D}_e^{-1}.$$

B. Reduced dissipative models

A dissipative static model of the planetary gear can be obtained from the extended model (4) when stiffness coefficients K_{cr} and K_{sc} tend to infinity and inertias go to zero $J_s = J_c = J_p = J_r = 0$, that is when $\overline{\mathbf{L}} = 0$:

$$\overline{\mathbf{x}} = \overline{\mathbf{A}}^{-1}\, \overline{\mathbf{B}}\, \mathbf{u}, \quad \rightarrow \quad \mathbf{y} = \overline{\mathbf{D}}\, \mathbf{u} = \overline{\mathbf{B}}^{\mathrm{T}}\, \overline{\mathbf{A}}^{-1}\, \overline{\mathbf{B}}\, \mathbf{u}. \tag{9}$$

Matrix $\overline{\mathbf{D}}$ is singular and therefore all the torque vectors $\mathbf{u} = [\tau_s, \tau_c, \tau_r]^{\mathrm{T}}$ which belong to the kernel of matrix $\overline{\mathbf{D}}$, i.e. which are parallel to vector $\mathbf{k}_1 = [r_s, -r_r - r_s, r_r]^{\mathrm{T}}$, do not influence the output velocities $\mathbf{y} = [\omega_s, \omega_c, \omega_r]^{\mathrm{T}}$. Moreover, all the velocities $\mathbf{y}$ obtained from (9) are perpendicular to vector $\mathbf{k}_1$, i.e. the vector $\mathbf{y}$ satisfies the relation:

$$\mathbf{k}_1^{\mathrm{T}}\, \mathbf{y} = 0 \quad \leftrightarrow \quad r_s\, \omega_s - (r_r + r_s)\, \omega_c + r_r\, \omega_r = 0. \tag{10}$$

IV. Electrical motors modeling

In this paper we refer to a permanent magnet synchronous motor (PMSM) with an *odd* number m_s of star-connected phases [10] characterized by the parameters shown in Tab. I.

m_s	number of motor phases;
p	number of polar expansions;
θ, θ_m	electric and rotor angular positions: $\theta = p\,\theta_m$;
ω, ω_m	electric and rotor angular velocities: $\omega = p\,\omega_m$;
R_s	i-th stator phase resistance;
L_s	i-th stator phase self induction coefficient;
M_{s0}	maximum value of mutual inductance between stator phases;
φ_c	maximum value of function $\phi_c(\theta)$;
J_m	rotor moment of inertia;
b_m	rotor linear friction coefficient;
τ_m	electromotive torque acting on the rotor;
τ_s	external load torque acting on the rotor;
γ_s	basic angular displacement ($\gamma_s = 2\pi/m_s$)

Table I
PARAMETERS OF THE MULTI-PHASE SYNCHRONOUS MOTOR.

Let us introduce the following current and voltage stator vectors:

$$ {}^t\mathbf{I}_s = \underset{1:m_s}{^{h}[\![\, I_{sh} \,]\!]},\ {}^t\mathbf{V}_s = \underset{1:m_s}{^{h}[\![\, V_{sh} \,]\!]} \tag{11} $$

where the following notation is used:

$$ \underset{1:n}{^{i}}\underset{1:m}{^{j}}[\![\, a_{i,j} \,]\!] = \begin{bmatrix} a_{11} & a_{12} & \cdots & a_{1m} \\ a_{21} & a_{22} & \cdots & a_{2m} \\ \vdots & \vdots & \ddots & \vdots \\ a_{n1} & a_{n2} & \cdots & a_{nm} \end{bmatrix}. $$

Let define the inductance matrix ${}^t\mathbf{L}_s$ as follows:

$$ {}^t\mathbf{L}_s = L_{s0}\,\mathbf{I}_{m_s} + M_{s0}\,\underset{1:m_s}{^{i}[\![\cos((i-j)\gamma_s)]\!]}\underset{1:m_s}{^{j}} $$

with $L_{s0} = L_s - M_{s0}$. The resistance matrix is ${}^t\mathbf{R}_s = R_s\,\mathbf{I}_{m_s}$ and we consider a periodic rotor flux function $\bar{\phi}(\theta)$ expressed in Fourier series as: $\bar{\phi}(\theta) = \sum_{n=1:2}^{m_s-2} a_n \cos(n\theta)$. Using a "Lagrangian" approach, see [9], and applying transformation ${}^t\mathbf{I}_s = {}^{\omega}\mathbf{T}_t^{\mathrm{T}}\,{}^{\omega}\mathbf{I}_s$ where the transformation matrix is:

$$ {}^{\omega}\mathbf{T}_t(\theta) = \sqrt{\frac{2}{m_s}}\underset{1:2:m_s-2}{^{k}\left\|\begin{bmatrix} \cos(k\,(\theta - h\,\gamma_s)) \\ \\ \sin(k\,(\theta - h\,\gamma_s)) \end{bmatrix}\right\|}\underset{0:m_s-1}{^{h}} \tag{12} $$

the dynamic equations of the electric motor in the transformed rotating frame Σ_ω are obtained:

$$ \left[\begin{array}{c|c} {}^{\omega}\mathbf{L}_s & 0 \\ \hline 0 & J_m \end{array}\right]\begin{bmatrix} {}^{\omega}\dot{\mathbf{I}}_s \\ \dot{\omega}_m \end{bmatrix} = -\left[\begin{array}{c|c} {}^{\omega}\mathbf{R}_s + {}^{\omega}\mathbf{L}_s\,{}^{\omega}\mathbf{J}_s & {}^{\omega}\mathbf{K}_\tau(\theta) \\ \hline -\,{}^{\omega}\mathbf{K}_\tau^{\mathrm{T}}(\theta) & b_m \end{array}\right]\begin{bmatrix} {}^{\omega}\mathbf{I}_s \\ \omega_m \end{bmatrix} + \begin{bmatrix} {}^{\omega}\mathbf{V}_s \\ -\tau_e \end{bmatrix} \tag{13} $$

where ${}^{\omega}\mathbf{L}_s = {}^t\mathbf{T}_\omega^{\mathrm{T}}\,{}^t\mathbf{L}_s\,{}^t\mathbf{T}_\omega$, ${}^{\omega}\mathbf{R}_s = {}^t\mathbf{R}_s$, ${}^{\omega}\mathbf{J}_s = {}^t\mathbf{T}_\omega^{\mathrm{T}}\,{}^t\dot{\mathbf{T}}_\omega$ and ${}^{\omega}\mathbf{V}_s = {}^t\mathbf{T}_\omega^{\mathrm{T}}\,{}^t\mathbf{V}_s$. Matrices ${}^{\omega}\mathbf{L}_s$ and ${}^{\omega}\mathbf{J}_s$ have the following diagonal structure:

$$ {}^{\omega}\mathbf{L}_s = \begin{bmatrix} L_{se} & 0 & 0 & \cdots & 0 \\ 0 & L_{se} & 0 & \cdots & 0 \\ 0 & 0 & L_{s0} & \cdots & 0 \\ \vdots & \vdots & \vdots & \ddots & \vdots \\ 0 & 0 & 0 & \cdots & L_{s0} \end{bmatrix}, \quad {}^{\omega}\mathbf{J}_s = \underset{1:2:m_s-2}{^{k}\left\|\begin{bmatrix} 0 & -k\,\omega \\ k\,\omega & 0 \end{bmatrix}\right\|}, $$

where $L_{se} = L_{s0} + \frac{m_s}{2}M_{s0}$ and $\omega = \dot{\theta}$. For the considered rotor flux $\bar{\phi}(\theta)$, the torque vector ${}^{\omega}\mathbf{K}_\tau(\theta)$ is constant, see [8], with the following expression:

$$ {}^{\omega}\mathbf{K}_\tau = -\varphi_c\,p\,\sqrt{\frac{m_s}{2}}\underset{1:2:m_s-2}{^{k}\left\|\begin{bmatrix} 0 \\ k\,a_k \end{bmatrix}\right\|} \tag{14} $$

Note that using this transformation the original state space Σ_t has been transformed into $(m_s-1)/2$ two-dimensional orthogonal subspaces and the m_s-phase machine can be seen as $(m_s-1)/2$ two-dimensional machines. The POG block scheme of the synchronous motor in the transformed space Σ_ω, see eq. (13), is shown in Fig. 7. The torque control of the

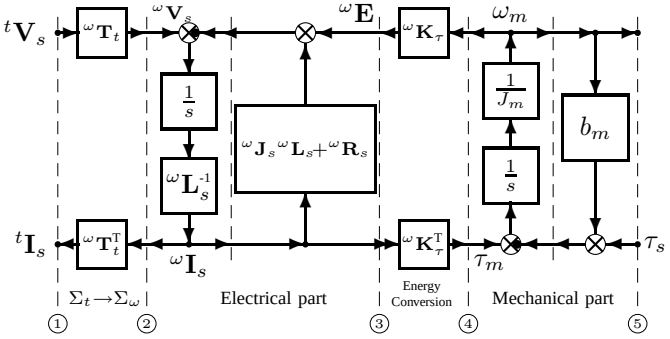

Figure 7. POG scheme of the PMSM in the transformed space Σ_ω.

PMSM is realized by the following control law:

$$ {}^{\omega}\mathbf{V}_s = ({}^{\omega}\mathbf{R}_s + {}^{\omega}\mathbf{J}_s\,{}^{\omega}\mathbf{L}_s)\,{}^{\omega}\mathbf{I}_s + {}^{\omega}\mathbf{K}_\tau\,\omega_m - \mathbf{K}_c({}^{\omega}\mathbf{I}_s - {}^{\omega}\mathbf{I}_d) \tag{15} $$

where ${}^{\omega}\mathbf{I}_d$ is the constant desired current and $\mathbf{K}_c > 0$ is a diagonal matrix used for the tuning of the control, see [10].

V. POG MODELING OF A HYBRID AUTOMOTIVE SYSTEM

The considered power-split architecture is shown in Fig. 8: it includes an internal combustion engine (ICE), a multi-phase Permanent Magnet Synchronous Machine (PMSM) and the vehicle [4]. The ICE is rigidly connected to the Carrier (C), the PMSM to the Sun (S) and the vehicle driving axle to the Ring (R). This hybrid system can be represented by the "high level"

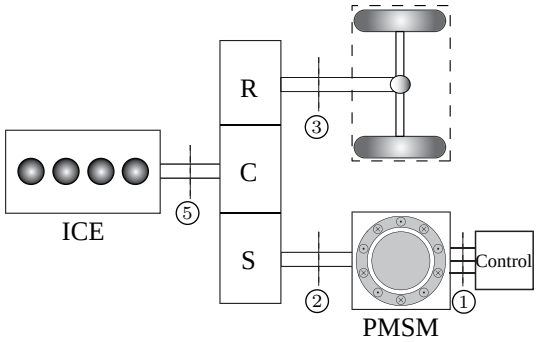

Figure 8. Scheme of the considered power structure of the vehicle

POG block scheme of Fig. 9 where power sections ① - ⑤ correspond to the physical power sections indicated in Fig. 8.

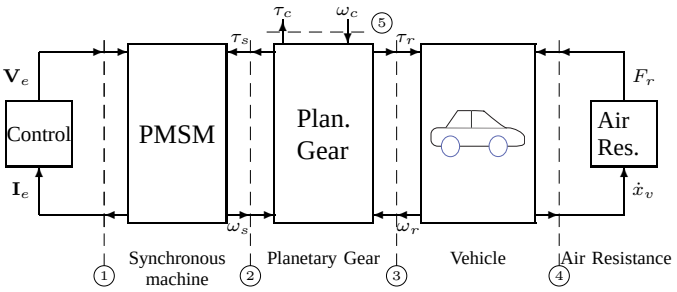

Figure 9. POG graphical representation of the considered hybrid vehicle.

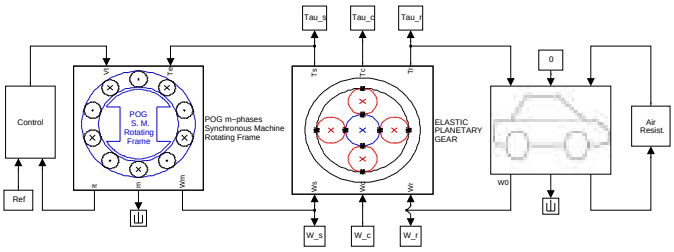

Figure 10. Simulink block scheme of the considered hybrid power structure.

The block "Control" in Fig. 9 represents the electric PMSM control. The POG model of the PMSM between sections ① and ② is given in Fig. 7, see [8] and [9]. The POG model of the planetary gear between sections ② and ③ is the elastic model given in Fig. 6. In ③ the Ring is connected to the driving shaft of the vehicle. The dynamics of the vehicle is described by the POG model between sections ③ and ④ , see [2] for details. Finally, last POG block describes the resistance of the air $F_r = F_r(\dot{x}_v)$.

VI. Simulation of the Hybrid Propulsion System

The presented hybrid propulsion system has been implemented in Matlab/Simulink and the obtained Simulink scheme is shown in Fig. 10. The "start-and-stop" simulation results reported in Fig. 11÷14 have been obtained with the ICE switched off, i.e. $\omega_c = 0$, and controlling the multi-phase electric motor in order to make the vehicle speed follow the trapezoidal velocity shape $\dot{x}_d$ shown in Fig. 11 (red dashed line). The velocity $\dot{x}_v$ of the vehicle follows $\dot{x}_d$ with a small delay because of the elastic horizontal slipping of the tires on the ground. Main parameters of the vehicle: $M_v = 1272$ kg vehicle mass; $J_w = 3.459$ kg m^2 wheels inertia; $R_w = 32.55$ cm wheels radius; $K_t = 360000$ N/m tires longitudinal stiffness. The angular velocities and torques of the planetary gear are shown in Fig. 12. Parameters of the planetary gear: $r_s = 10.2$ cm, $r_r = 24.8$ cm, $K_{sc} = K_{cr} = 10^7$ N/m, $d_{sc} = d_{cr} = 3003$ N s/m, $J_p = 0.0812$ kg m^2, $[b_p, b_s, b_c, b_r] = [0.243, 0.148, 2.787, 6.541]$ N m/rad. Voltages $\mathbf{V}_e$ and currents $\mathbf{I}_e$ of the 5-phase PMSM are shown in Fig. 13. Parameters of the PMSM with sinusoidal flux: $R_s = 1\ \Omega$, $L_s = 0.01$ H, $M_{s0} = 0.008$ H, $\varphi_c = 6$ W, $J_m = 0.529$ kg m^2, $b_m = 0.08$ N m s/rad. The power flows within the system are shown in Fig. 14: P_1 power in section ① (from the control unit towards the electric motor),

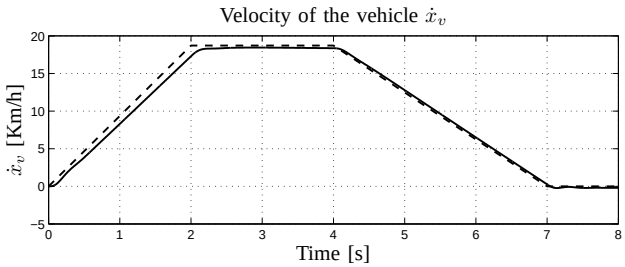

Figure 11. Velocity of the vehicle $\dot{x}_v$ (blue, solid) compared with the desired velocity $\dot{x}_d$ (red, dashed).

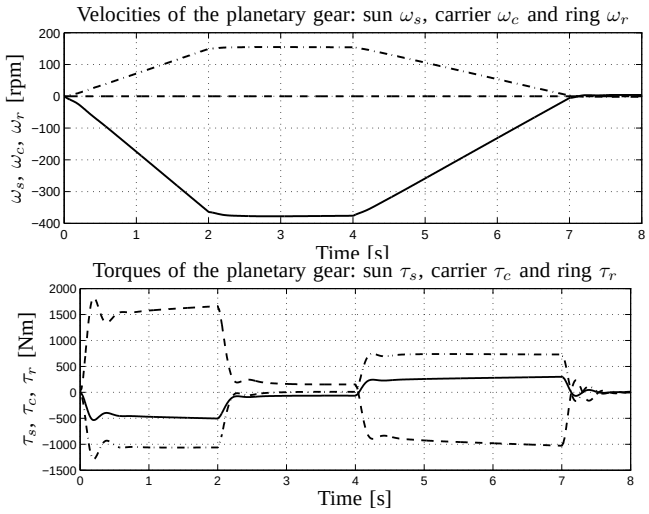

Figure 12. Velocities and torques of the planetary gear: sun ω_s (red, solid), carrier ω_c (blue, dashed) and ring ω_r (black, dash-dotted).

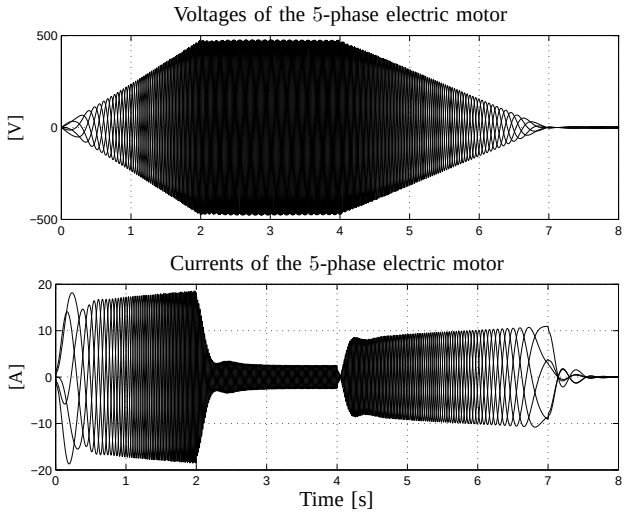

Figure 13. Voltages $\mathbf{V}_e$ and currents $\mathbf{I}_e$ of the 5-phase electric motor.

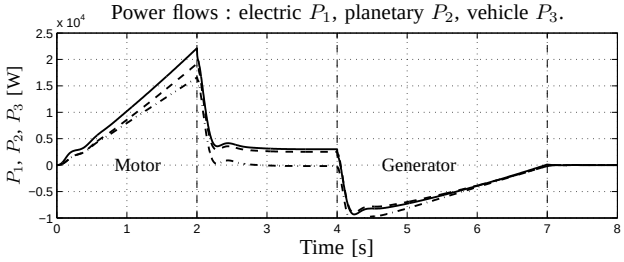

Figure 14. Powers entering the subsystems: P_1 electric motor (red, plain), P_2 planetary gear (blue, dashed), P_3 vehicle (black, dash-dotted).

P_2 mechanical power in section ② (from the electrical motor towards the planetary gear), P_3 mechanical power in section ③ (towards the vehicle). When $t \in [0, 2]$ s the vehicle accelerates and part of the power flowing towards the vehicle dissipates within the electric motor and within the planetary gear. When $t \in [4, 7]$ s the vehicle decelerates and an amount of mechanical power flows from the vehicle towards the electric motor thus acting as generator, see Fig. 14.

VII. Conclusions

In this paper a power-split hybrid electric vehicle is modeled using the Power-Oriented Graphs technique. The main subsystems (internal combustion engine, multi-phase synchronous motor, planetary gear and vehicle dynamics) are modelled taking advantages from the main features of POG such as the possibility to reduce and transform systems. Simulations results show the effectiveness of the proposed models.

References

[1] K. Chen, W. Lhomme, A. Bouscayrol, A. Berthon "Comparison of two series-parallel Hybrid Electric Vehicles focusing on control structures and operation modes" Vehicular Power and Propulsion Conference VPPC 2009, Dearborn, Michigan, USA 7-11 september 2009

[2] F. Grossi, W. Lhomme, R. Zanasi, A. Bouscayrol, "Modelling and control of a vehicle with tire-road interaction using POG and EMR formalisms", accepted to Electromotion 2009, EPE chapter Electric Drives, 1-3 July 2009, Lille, France

[3] D. C. Karnopp, D.L. Margolis, R. C. Rosemberg, *System dynamics - Modeling and Simulation of Mechatronic Systems*, Wiley Interscience, ISBN 0-471-33301-8, 3rd ed. 2000.

[4] Miller, J.M., "Hybrid Electric Vehicle Propulsion System Architectures of the e-CVT Type", IEEE Transactions On Power Electronics, Vol. 21, No. 3, May 2006.

[5] Paynter, H.M., *Analysis and Design of Engineering Systems*, MIT-press, Camb., MA, 1961.

[6] Wenyong Li; A. Abel, K. Todtermuschke,Tong Zhang "Hybrid Vehicle Power Transmission Modeling and Simulation with SimulationX" International Conference on Mechatronics and Automation, ICMA 2007.

[7] R. Zanasi, "Power Oriented Modelling of Dynamical System for Simulation", IMACS Symp. on Modelling and Control of Technological System, Lille, France, May 1991.

[8] R. Zanasi, F. Grossi, "Multi-phase Synchronous Motors: POG Modeling and Optimal Shaping of the Rotor Flux", ELECTRIMACS 2008, Québec, Canada, June 2008.

[9] R. Zanasi, F. Grossi "Optimal Rotor Flux Shape for Multi-phase Permanent Magnet Synchronous Motors", International Power Electronics and Motion Control Conference, September 1-3 2008, Poznan, Poland.

[10] R. Zanasi, F. Grossi, "Vectorial Control of Multi-phase Synchronous Motors using POG Approach", IECON 2009, 35th Annual Conference of the IEEE Industrial Electronics Society, November 3-5, 2009 Porto, Portugal.

[11] R.Zanasi, F.Grossi "The POG Technique for Modeling Planetary Gears and Hybrid Automotive Systems" Vehicular Power and Propulsion Conference VPPC 2009, Dearborn, Michigan, USA 7-11 september 2009